Unified Formulation for Compressible-Incompressible Flow Simulation with Mesh Adaptation

É. Turgeon* and D. Pelletier†
École Polytechnique de Montréal, Montréal, Québec H3C 3A7, Canada

Introduction

MANY computational fluid dynamics (CFD) problems are characterized by flows that are incompressible in most of the domain with embedded regions where compressibility effects are significant and cannot be neglected. Examples include airfoils at takeoff conditions, leaks from pressurized tanks, and anti-icing devices such as Picolo tubes. Viscous flows spanning this range of compressibility are notoriously difficult to solve with density-based methods as the continuity and energy equations present indeterminacies in the limit of vanishing Mach number [see Eq. (4)].[1] Preconditioning of density-based equations has met with better success for inviscid flows than for viscous flows. An alternative is to extend an incompressible pressure-based formulation to the compressible flow regime.[2,3] This Note proposes a pressure-based formulation capable of handling compressible and incompressible flows. The approach is general and applicable to both viscous and inviscid flows and to cases with variable fluid properties.[3,4]

Modeling of the Problem

The flow regime of interest is steady, laminar, and compressible, with variable fluid properties, and includes heat-transfer effects. It is modeled by the continuity, Navier–Stokes, and energy equations

$$-\nabla\cdot\boldsymbol{u} = (1/\rho)\boldsymbol{u}\cdot\nabla\rho$$

$$\rho\boldsymbol{u}\cdot\nabla\boldsymbol{u} = -\nabla p + \nabla\cdot\left[\mu(\nabla\boldsymbol{u}+\nabla\boldsymbol{u}^T) - \tfrac{2}{3}\mu\boldsymbol{I}\,\nabla\cdot\boldsymbol{u}\right] + \rho\boldsymbol{f}$$

$$\rho c_p\boldsymbol{u}\cdot\nabla T = \boldsymbol{u}\cdot\nabla p + \nabla\cdot(\lambda\nabla T) + \rho q_s \qquad (1)$$

where $\boldsymbol{u}$ is the velocity, ρ the density, p the pressure, μ the fluid viscosity, $\boldsymbol{I}$ the identity matrix, $\boldsymbol{f}$ a body force, c_p the specific heat at constant pressure, T the temperature, λ the thermal conductivity, and q_s a heat source. The fluid properties μ, c_p, and λ are either constant or temperature dependent. The temperature dependence used here is given in Table 1. These relationships correspond to the correlations suggested by Aihara et al.,[5] which are valid between 280 and 650 K. Finally, the subscript r denotes a reference state. The perfect gas equation of state closes the system:

$$\rho = p/RT \qquad (2)$$

In this expression R is the thermodynamic constant of the gas. Dirichlet and Neumann boundary conditions complete the statement of the problem.

A pressure-based finite element method is used to solve the preceding equations. Hence only velocity, pressure, and temperature are discretized. Density is evaluated through the equation of state. Thus, the continuity equation can be written as

$$-\nabla\cdot\boldsymbol{u} = (1/p)\boldsymbol{u}\cdot\nabla p - (1/T)\boldsymbol{u}\cdot\nabla T \qquad (3)$$

Table 1 Temperature dependence of air properties

Property	Dependence
c_p/c_{p_r}	$(T/T_r)^{0.05}$
μ/μ_r	$(T/T_r)^{0.68}$
λ/λ_r	$(T/T_r)^{0.76}$

Although mathematically correct, this form of the equations yields indeterminacies in the limit case of vanishing Mach number. A nondimensional form of the equations can shed light on this issue.

We seek a nondimensional formulation, free of indeterminacies, suitable for all flow regimes: compressible [$\rho=\rho(p,T)$], anelastic flows [$\rho=\rho(T)$], and ($\rho=$ constant). Our starting point is the usual dimensionless form used in aerodynamics:

$$\tilde{x} = x/L_r, \qquad \tilde{T} = T/T_r, \qquad \tilde{\rho} = \rho/\rho_r, \qquad \tilde{\mu} = \mu/\mu_r$$

$$\tilde{\boldsymbol{u}} = \boldsymbol{u}/U_r, \qquad \tilde{p} = p/p_s, \qquad \tilde{c}_p = c_p\big/c_{p_r}, \qquad \tilde{\lambda} = \lambda/\lambda_r$$

where $p_s=\rho_r U_r^2$ is a pressure scale. The subscript r stands for a reference state, typically the freestream conditions. This yields the following nondimensional system:

$$-\tilde{\nabla}\cdot\tilde{\boldsymbol{u}} = (1/\tilde{p})\tilde{\boldsymbol{u}}\cdot\tilde{\nabla}\tilde{p} - (1/\tilde{T})\tilde{\boldsymbol{u}}\cdot\tilde{\nabla}\tilde{T}$$

$$\tilde{\rho}\tilde{\boldsymbol{u}}\cdot\tilde{\nabla}\tilde{\boldsymbol{u}} = -\tilde{\nabla}\tilde{p} + (1/Re)\tilde{\nabla}\cdot\left[\tilde{\mu}(\tilde{\nabla}\tilde{\boldsymbol{u}}+\tilde{\nabla}\tilde{\boldsymbol{u}}^T) - \tfrac{2}{3}\tilde{\mu}\boldsymbol{I}\,\tilde{\nabla}\cdot\tilde{\boldsymbol{u}}\right] + \tilde{\rho}\tilde{\boldsymbol{f}}$$

$$\tilde{\rho}\tilde{c}_p\tilde{\boldsymbol{u}}\cdot\tilde{\nabla}\tilde{T} = (\gamma_r-1)M_r^2\tilde{\boldsymbol{u}}\cdot\tilde{\nabla}\tilde{p} + (1/Re\,Pr)\tilde{\nabla}\cdot(\tilde{\lambda}\tilde{\nabla}\tilde{T}) + \tilde{\rho}\tilde{q}_s$$

$$\tilde{\rho} = \gamma_r M_r^2(\tilde{p}/\tilde{T}) \qquad (4)$$

where

$$Re = \frac{\rho_r U_r L_r}{\mu_r}, \qquad Pr = \frac{\mu_r c_{p_r}}{\lambda_r}, \qquad M_r = \frac{U_r}{\sqrt{\gamma_r RT_r}}$$

These equations are well suited for compressible flows, but they exhibit problems in the limit of vanishing Mach number. One might mistakenly conclude from the equation of state that density goes to zero as the Mach number vanishes while, in fact, the appropriate conclusion is that pressure behaves as the inverse of the Mach number squared.

This apparent indeterminacy is caused by an improper nondimensionalization of pressure. Here, the pressure scale is

$$p_s = \rho_r U_r^2 = \gamma_r p_r M_r^2$$

which is representative of pressure differences in the flow. Thus, we have

$$\Delta p/p_r \sim M_r^2$$

Hence, very-low-Mach-number flows experience pressure differences which are much smaller than the absolute or thermodynamic pressure. This illustrates the dual role of pressure: the absolute pressure plays a thermodynamic role in the equation of state while pressure differences play a mechanical role in the momentum equations. The present pressure scaling ensures that the magnitude of the dimensionless pressure differences is of the order one. However, the dimensionless absolute pressure itself goes to infinity as the reference Mach number approaches zero. An appropriate nondimensionalization for the pressure should provide magnitudes of order one for both the dimensionless pressure differences in the momentum equation and the dimensionless thermodynamic pressure in the equation of state. Meeting these conditions will improve the behavior of the numerical solution algorithm and will ensure that the appropriate limiting form of the equations are recovered without indeterminacies.

This is achieved by selecting appropriate values for both the reference state ($p_r T_r$) and the scale for pressure and temperature ($p_s T_s$):

$$\tilde{p} = (p-p_r)/p_s = (p-p_r)\big/\rho_r U_r^2, \qquad \tilde{T} = (T-T_r)/T_s$$

Presented as Paper 99-0875 at the AIAA 37th Aerospace Sciences Meeting, Reno, NV, 11–14 January 1999; received 22 April 2000; revision received 19 July 2001; accepted for publication 31 July 2001.

*Graduate Student, Département de Génie Mécanique.
†Professor, Canada Research Chair in Multidisciplinary Analysis, Département de Génie Mécanique. Associate Fellow AIAA.

Equations (1–3) then take the following form:

$$-\tilde{\nabla}\cdot\tilde{\boldsymbol{u}} = \frac{\gamma_r M_r^2}{\gamma_r M_r^2\tilde{p}+1}\tilde{\boldsymbol{u}}\cdot\tilde{\nabla}\tilde{p} - \frac{T_s/T_r}{(T_s/T_r)\tilde{T}+1}\tilde{\boldsymbol{u}}\cdot\tilde{\nabla}\tilde{T}$$

$$\tilde{\rho}\tilde{\boldsymbol{u}}\cdot\tilde{\nabla}\tilde{\boldsymbol{u}} = -\tilde{\nabla}\tilde{p} + \frac{1}{Re}\tilde{\nabla}\cdot\left[\tilde{\mu}(\tilde{\nabla}\tilde{\boldsymbol{u}}+\tilde{\nabla}\tilde{\boldsymbol{u}}^T) - \frac{2}{3}\tilde{\mu}\boldsymbol{I}\,\tilde{\nabla}\cdot\tilde{\boldsymbol{u}}\right] + \tilde{\rho}\tilde{\boldsymbol{f}}$$

$$\tilde{\rho}\tilde{c}_p\tilde{\boldsymbol{u}}\cdot\tilde{\nabla}\tilde{T} = Ec\;\tilde{\boldsymbol{u}}\cdot\tilde{\nabla}\tilde{p} + \frac{1}{Re\,Pr}\tilde{\nabla}\cdot(\tilde{\lambda}\tilde{\nabla}\tilde{T}) + \tilde{\rho}\tilde{q}_s$$

$$\tilde{\rho} = \frac{\gamma_r M_r^2\tilde{p}+1}{(T_s/T_r)\tilde{T}+1} \tag{5}$$

where Ec is the Eckert number:

$$Ec = \frac{(\gamma_r-1)M_r^2}{T_s/T_r}$$

Equations (5) are applicable to fully compressible flows. They yield the appropriate low-Mach-number equations in the limit of $M_r = 0$, which implies $Ec = 0$. These are the so-called anelastic flow equations.[6] They also yield the incompressible flow form of the Navier–Stokes equations when temperature differences are small ($T_s/T_r = 0$).

The only possible anomaly is the presence of the term $\frac{2}{3}\tilde{\mu}\boldsymbol{I}\,\tilde{\nabla}\cdot\tilde{\boldsymbol{u}}$. But because the continuity equation requires a divergence free velocity vector, this term will numerically vanish. Thus the appropriate incompressible flow equations are recovered. Finally, the limit ($T_s/T_r = 0$) yields

$$T/T_r = \tilde{T}(T_s/T_r) + 1 = 1$$

so that fluid properties (Table 1) are constant as expected:

$$\tilde{\mu} = \mu/\mu_r = 1, \qquad \tilde{\lambda} = \lambda/\lambda_r = 1, \qquad \tilde{c}_p = c_p/c_{p_r} = 1$$

The simultaneous limits $M_r = 0$ and $T_s/T_r = 0$ generate an indeterminacy for Ec. This special case must be studied carefully because the two limits ($M_r = 0$ and $T_s/T_r = 0$) are independent processes. The Eckert number is

$$(\gamma_r-1)M_r^2 T_r/T_s \to 0/0 \tag{6}$$

The physical interpretation of this term provides the basis to properly specify the input parameter, that is, $Ec = 0$. For adiabatic walls the temperature scale (the typical temperature differences) is that described by Panton[1]:

$$\Delta T_{\text{adiabatic}} \sim U_r^2/c_{p_r} = (\gamma_r-1)T_r M_r^2$$

This is the numerator of Eq. (6). Hence, the Eckert number can symbolically be written as

$$Ec = \frac{\Delta T_{\text{adiabatic}}}{\Delta T_{\text{imposed}}}$$

When the flow approaches incompressibility, T_s must be small to ensure that fluid properties are constant. Hence, $\Delta T_{\text{imposed}}$ is small. At the same time $\Delta T_{\text{adiabatic}}$ must be much smaller than $\Delta T_{\text{imposed}}$ to guarantee that temperature changes and heat transfer are driven by the prescribed Dirichlet condition and not by compressibility effects. This is accomplished by setting $Ec = 0$ in Eqs. (5) so that the usual incompressible flow equations are recovered.

In summary, the proposed formulation using appropriate scales and reference states for both temperature and pressure makes it possible to treat all flow regimes in a unified manner: fully compressible, anelastic, and incompressible. A single system of differential equations (5) is used, and the input parameters (M_r, Ec, and T_s/T_r) define the specific flow regime.

Adaptive Finite Element Method

The problem is solved using a standard Galerkin finite element method. The variational equations are obtained by multiplying each equation by a test function and integrating over the computational domain. The pressure gradient and viscous conduction terms are integrated by parts to provide natural boundary conditions. The weak form is detailed in our previous work.[3,4] The system of equations is fully coupled and highly nonlinear, especially when density and properties vary. The continuity-momentum-energy system is solved in a fully coupled manner, using Newton's method. The discretization uses a quadratic velocity field, a quadratic temperature, and a linear continuous pressure approximation on each finite element.

The adaptive remeshing procedure is modeled after that of Peraire et al.[7] and is described in more details by Ilinca and Pelletier.[3] The procedure clusters grid points in regions of rapid variations of all dependent variables. Error estimates are obtained for velocity, pressure and temperature by a local least-squares reconstruction of the solution derivatives.[8,9] Following Ilinca and Pelletier,[3] we consider the temperature derivatives and not the conduction fluxes. We omit the diffusion coefficient because properties vary with temperature so that element diffusion fluxes are no longer linear functions. For the velocity field, the term $\tilde{\nabla}\tilde{\boldsymbol{u}}+\tilde{\nabla}\tilde{\boldsymbol{u}}^T - \frac{2}{3}\boldsymbol{I}\,\tilde{\nabla}\cdot\tilde{\boldsymbol{u}}$ is used for error estimation. An error estimate for pressure is obtained by a local projection of the pressure itself. No explicit error estimate is computed for density. Because density is computed via the equation of state, its accuracy is controlled by that of pressure and temperature.

Once the error estimates are obtained for all variables (velocity, temperature and temperature), a better mesh must be designed. In our approach all variables are analyzed and contribute to the mesh adaptation process. For this an error estimate is obtained separately for each dependent variable. The mesh characteristics (element size) on a given element are derived for each variable by equidistribution of the error.[7] The minimum element size predicted for each of the dependent variable is selected on each element. Details of this algorithm have been presented previously.[3]

Applications

Turgeon et al.[4] verified the adaptive finite element method on a problem with a closed-form solution. The problem is designed to mimic a compressible laminar round jet impinging on a heated flat plate. The variable fluid properties for air in Table 1 are used. See Turgeon et al.[4] for details. For this problem both the error estimate and the true error can be computed and compared. Results show that mesh adaptation improves the accuracy of boh the solution and the error estimator. Furthermore, results show that mesh adaptation leads to grid-independent predictions of both skin friction and Nusselt number along the solid wall. Figure 1 illustrates the mesh convergence of the Nusselt number.

Next, the formulation is applied to the air jet of Aihara et al.[5] Figure 2 presents skin-friction distribution along the solid wall for five cases. The first three cover incompressible flow with constant properties, a cold compressible jet on a hot wall, and a hot compressible jet on a cold wall. In addition, the effect of variable density is investigated by performing two additional simulations: one has variable density and constant physical properties, whereas the other is

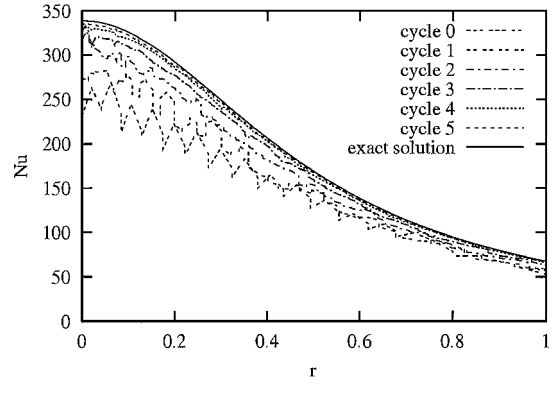

Fig. 1 Analytical jet: Nusselt number.

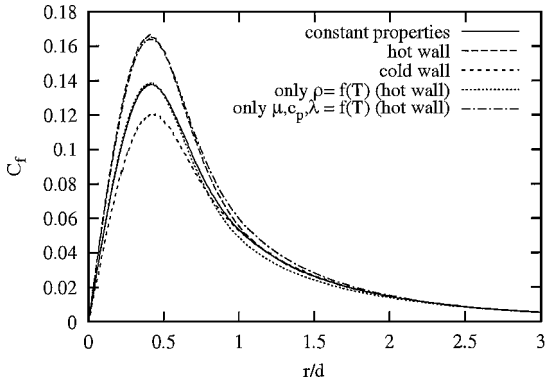

Fig. 2 Skin friction for air.

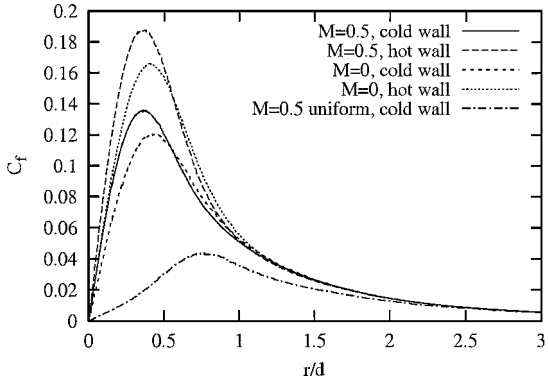

Fig. 3 Air at $M = 0.5$: skin friction.

for incompressible flow (constant density) with variable physical properties. As can be seen, the wall conditions have the most pronounced influence of the distribution of skin friction. C_f is larger when the jet is heated by the wall because the viscosity of air increases with temperature. In fact, if one looks at the cases of constant density and of constant physical properties, one concludes that the effect of ρ is small but that those of the other properties is larger. Incompressible and compressible jets with constant properties are almost identical, whereas predictions from variable property models for a hot wall are extremely close together.

Next, complexity of the problem is increased by including compressibility effects caused by pressure (Mach number effects). The preceding problem is solved again, but this time with $M_r = 0.5$. This choice deserves some comments. First, the Reynolds number is kept at 500. This condition will occur for very small geometries (small length scale L_r). It also allows for a direct comparison with low-Mach-number results. Also, the inlet velocity profile is again parabolic. It is realistic even at high subsonic M_r because the Reynolds number is low (important viscous effects). The reference velocity is the mean inlet velocity, thus the inlet Mach-number distribution is parabolic with a maximum of one. Finally, the inlet tube is reduced to a smaller length $(0.2d)$ to avoid temperature drops, which would make comparisons to low-Mach-number solutions more difficult. The study is restricted to air. The governing equations are given by system (5), and the fluid properties vary according to the expressions given in Table 1. Figure 3 provides the local skin-friction coefficient distribution along the wall. Compressibility increases the level of C_f for both cases. The location of the maximum is also closer to the axis of symmetry. Including compressibility effects also increases the demands on the flow solver. Compressibility increases the velocity and temperature gradients at the wall, thus making the problem more difficult to solve in terms of nonlinearities and mesh refinement. The cold-wall problems are also more demanding. The air conductivity $\tilde{\lambda}_w$ is lower for a cold wall than for a hot wall. Hence, the temperature gradient at the wall is larger for the cold wall than the hot wall. The hydrodynamic boundary layer is also thinner for a cold wall because the apparent viscosity is lower. For example, $\tilde{\nabla}\tilde{T}$ is five times higher for the air jet on a cold wall at $M_r = 0.5$ than for the air jet on a hot wall at $M_r = 0$.

Conclusions

A unified formulation of the flow equations was presented to treat three flow regimes: incompressible flow, strongly heated flow, and fully compressible flow. A flow solver using this formulation can handle the simultaneous presence of these regimes in different parts of the domain as well as temperature-dependent fluid properties. Predictions for different flow regimes can be compared with confidence because the discretization is the same for all cases.

The adaptive finite element method yields grid-independent solution for all fields of interest: velocity, pressure, temperature, skin friction, and Nusselt number.

Computations for air illustrate the pronounced effect of the temperature dependence of fluid properties on the wall shear stress. Globally, C_f is higher for jets impinging on hot walls and are lower for cold walls. Jets at high subsonic Mach number show increases in C_f when compared to strongly heated low-Mach-number cases.

Acknowledgments

This work was supported in part by the National Science and Engineering Research Council, Fonds Cocerte d'Aide a la Recherche, and the Canada Research Chair Program.

References

[1]Panton, R. L., *Incompressible Flow*, Wiley-Interscience, New York, 1984, pp. 237–260.

[2]Tezduyar, T., Aliabadi, S., Behr, M., and Mittal, S., "Massively Parallel Finite Element Simulation of Compressible and Incompressible Flows," Army High Performance Computing Center, Rept. 94-013, Minneapolis, MN, Jan. 1994.

[3]Ilinca, F., and Pelletier, D., "A Unified Approach for Adaptive Solutions of Compressible and Incompressible Flow," AIAA Paper 97-0330, Jan. 1997.

[4]Turgeon, É., Pelletier, D., and Ilinca, F., "Compressible Heat Transfer Computations by an Adaptive Finite Element Method," AIAA Paper 99-0875, Jan. 1999.

[5]Aihara, T., Kim, J. K., and Maruyama, S., "Effects of Temperature-Dependent Fluid Properties on Heat Transfer Due to an Axisymmetric Impinging Gas Jet Normal to a Flat Surface," *Wärme- und Stoffübertragung*, Vol. 25, No. 1, 1990, pp. 145–153.

[6]Sherman, F. S., *Viscous Flow*, McGraw–Hill, New York, 1990, pp. 82, 83.

[7]Peraire, J., Vahdati, M., Morgan, K., and Zienkiewicz, O. C., "Adaptive Remeshing for Compressible Flow Computations," *Journal of Computational Physics*, Vol. 72, No. 2, 1987, pp. 449–466.

[8]Zienkiewicz, O. C., and Zhu, J. Z., "The Superconvergent Patch Recovery and a Posteriori Error Estimates. Part 1: The Recovery Technique," *International Journal for Numerical Method in Engineering*, Vol. 33, No. 7, 1992, pp. 1331–1364.

[9]Zienkiewicz, O. C., and Zhu, J. Z., "The Superconvergent Patch Recovery and A Posteriori Error Estimates. Part 2: Error Estimates and Adaptivity," *International Journal for Numerical Method in Engineering*, Vol. 33, No. 7, 1992, pp. 1365–1382.

J. Kallinderis
Associate Editor